# Batch-CAM: Introduction to better reasoning in convolutional deep learning models

Giacomo Ignesti<sup>1,2\*</sup>, Davide Moroni<sup>1†</sup> and Massimo Martinelli<sup>1†</sup>

<sup>1\*</sup>ISTI, CNR, Via Giuseppe Moruzzi, Pisa, 56124,Italy.

<sup>2\*</sup>Computer Science Department, University of Pisa, Street, City,

56123, Italy.

\*Corresponding author(s). E-mail(s): giacomo.ignesti@isti.cnr.it; Contributing authors: davide.moroni@isti.cnr.it; massimo.martinelli@isti.cnr.it; †These authors contributed equally to this work.

#### Abstract

Understanding the inner workings of deep learning models is crucial for advancing artificial intelligence, particularly in high-stakes fields such as healthcare, where accurate explanations are as vital as precision. This paper introduces Batch-CAM, a novel training paradigm that fuses a batch implementation of the Grad-CAM algorithm with a prototypical reconstruction loss. This combination guides the model to focus on salient image features, thereby enhancing its performance across classification tasks. Our results demonstrate that Batch-CAM achieves a simultaneous improvement in accuracy and image reconstruction quality while reducing training and inference times. By ensuring models learn from evidence-relevant information, this approach makes a relevant contribution to building more transparent, explainable, and trustworthy AI systems.

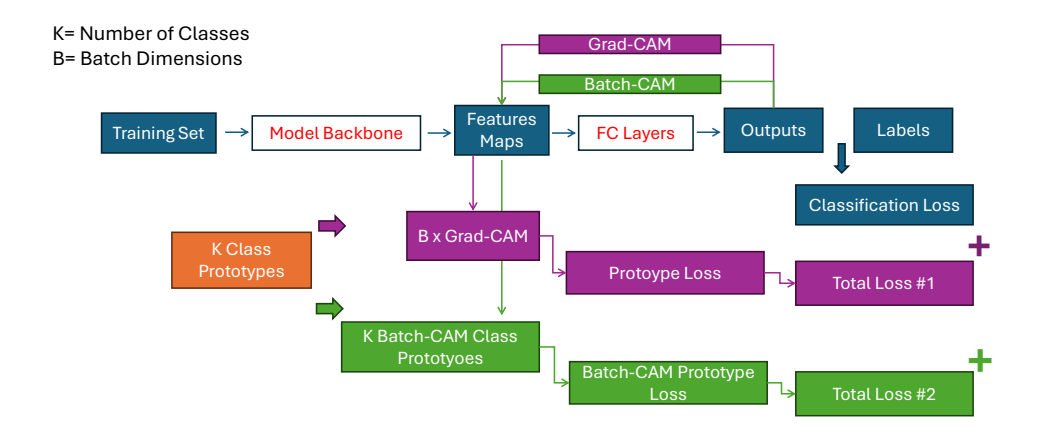
Keywords: AI, Batch, CAM, Deep Learning

# 1 Introduction

Although modern deep learning (DL) models for computer vision, notably Convolutional Neural Networks (CNNs) [1] and Vision Transformers (ViTs) [2], have demonstrated exceptional performance, their black-box nature fundamentally limits

our understanding of their decision-making processes. This opacity, a direct consequence of their intricate, non-linear optimisation, poses significant challenges for model interpretability, accountability, and safe deployment in high-stakes scenarios such as medical diagnostics, financial modelling, or autonomous driving. For instance, a model trained to detect pneumonia might achieve high accuracy by focusing on a hospital-specific pattern or insegna while being statistically effective on the training data. However, such a model would be erroneous when deployed in a new hospital [3]. The divergence between a model's high predictive accuracy and its lack of human-interpretable reasoning creates a critical gap that must be addressed for the broader, responsible adoption of Artificial Intelligence (AI). Artificial General Intelligence (AGI) exemplifies this challenge, aiming to develop models whose generalisation capabilities extend beyond their training domain, driven by an ability to simulate genuine thinking [4] and of the steps towards that it is represented by eXplainable Artificial Intelligence (XAI) that was explicitly developed to address this issue, creating techniques to make AI systems and their outputs more transparent and comprehensible, thereby fostering trust and exposing hidden vulnerabilities. The extensive development of XAI techniques [5] is just one possible approach to understanding AI and developing more robust models. Other approaches focus on designing novel model architectures and training paradigms that inherently enhance the reasoning and generalisation capabilities of DL. A modern example of this evolution is the emergence of Large Language Models (LLMs), which are predominantly built upon the Transformer architecture [6]. Unlike their predecessors, which were often designed for specific, narrow tasks, LLMs represent a shift towards more generalised intelligence.

This paper expands a novel training paradigm [7, 8] to enhance computer vision by integrating an explanatory mechanism into the learning process itself. Our core hypothesis is that the model already possesses sufficient information within the training data to be both precise and capable of generalisation, provided it is guided to focus on the correct features. We introduce a method that combines the Grad-CAM algorithm [9] with a tailored reconstruction loss term. This forces the model not only to classify an image correctly but also to detect which part of the image should get its focus. By comparing this generated explanation against a class prototype, our loss function provides evidence on which part of the image should be used to return the classification, effectively compelling it to learn for the right reasons. We extend this concept by exploring two innovative approaches: an image-to-prototype comparison to learn from a generalised class distribution and a Batch-CAM technique, where the model's averaged focus across a batch is regularised, as shown in Figure 1. These methods are evaluated using more robust distance metrics, including L1/L2 Loss and Structural Similarity Index SSIM Loss, to ensure meaningful comparisons. This paper introduces an improved training paradigm for supervised image classification. Section 2 explores the foundational concepts and related works that underpin our contribution. Section 3 details the evolution of our proposed architecture, explaining the algorithmic improvements and the different approaches investigated. Section 4 presents a comprehensive performance evaluation on several benchmark datasets, including MNIST and Fashion-MNIST, followed by an in-depth analysis of the results. Finally, Section



Total Loss #1 = Classification Loss + Protoype Loss
Total Loss #2 = Classification Loss + Batch-CAM Prototype Loss

 ${f Fig.~1}$  Proposed new model training protocol with both the prototype loss, and the Batch-CAM prototype loss

5 concludes by proposing future research directions that aim to extend and validate our approach in more complex domains.

#### 2 Foundations and Related Works

The challenge of creating trustworthy AI has inspired the development of a diverse range of interpretability techniques. Our work is situated at the intersection of three key research topics: post-hoc explanation methods that analyse trained models, intrinsically interpretable models designed for transparency, and training-time interventions that guide a model's learning process. These steps are achieved by manipulating the loss function, leveraging XAI algorithms, and utilising the training process efficiently.

#### 2.1 The Loss Function as a Control Mechanism

The loss function is the cornerstone of DL and Machine Learning (ML) models. It quantifies the difference between the model's prediction and the ground truth, and the entire training process is an optimisation problem aimed at minimising this value through backpropagation [10]. While standard loss functions like Cross-Entropy are staples for classification tasks [11], the increasing complexity of AI demands more sophisticated objective functions. Advanced models often employ a composite loss, combining multiple summands to enforce different constraints. For example, recent self-supervised models like DINOv3 use a combination of cross-entropy, a regulariser for feature space uniformity, and a novel objective to prevent feature degradation [12]. This demonstrates a powerful principle: the loss function can be augmented to do

more than guide accuracy; it can be engineered to shape the model's internal representations and behaviour. Another approach to loss control is presented in physical informed neural networks (PINNs) [13], in which the input data are correlated with the data through a bound in the loss term. The restraint can be a boundary condition of a hypothetical physical phenomenon whose violation would be impossible due to physical laws. PINNs have evolved far beyond solving simple forward problems; modern applications leverage them for complex inverse problems, such as discovering unknown physical parameters (e.g., fluid viscosity or material conductivity) from limited sensor data. They are now being applied to high-impact domains, including biomedical engineering (modelling blood flow and soft tissue mechanics), geophysics, and the creation of digital twins for industrial systems. This body of work, extensively reviewed by Karniadakis et al. in their 2021 Nature Reviews Physics paper [14], demonstrates the application of all this possible paradigm for imbuing models with robust domain knowledge.

# 2.2 Paradigms in Explainable AI

XAI methods can be broadly categorised by when and how they provide explanations. The two primary families are post-hoc techniques, which explain decisions after a model is trained, and intrinsically interpretable models, which are transparent by design. Post-hoc methods are the most common approach for interpreting existing black-box models. They operate by analysing a trained model to understand its behaviour for a specific input. One of the earliest and most influential methods is LIME (Local Interpretable Model-agnostic Explanations), which approximates the complex decision boundary of any model in the local vicinity of a prediction with a simpler, linear model [15]. In computer vision, attribution methods are dominant. These techniques generate saliency maps (or heatmaps) that highlight the pixels or regions of an input image most influential to the final prediction. Class Activation Map (CAM) and its widely used successors, Grad-CAM and Grad-CAM++ [16] are pioneering examples. Grad-CAM uses the gradients flowing into the final convolutional layer of a CNN to produce a coarse localisation map of the critical regions in the image. While incredibly useful for debugging and understanding what a model has learned, these methods share a fundamental limitation: they are purely diagnostic in nature. They can reveal that a model is relying on spurious correlations, but they offer no direct mechanism to correct it. In contrast to post-hoc analysis, this paradigm seeks to build models that are transparent by design. Instead of explaining a decision after the fact, the model's reasoning process is inherently understandable to humans. In computer vision, prototype-based networks are a prominent example [17]. These models learn a set of representative exemplar archetypes for each class during training. To make a prediction, the model compares parts of the input image to its learned prototypes and explains its decision by highlighting the similarities between these parts and the prototypes. This approach offers a powerful form of reasoning. Still, it can sometimes come at the cost of predictive performance and may be less flexible for tasks not easily broken down into part-based comparisons [18].

## 2.3 Guiding Models to Learn for the "Right Reasons"

A third possible paradigm synthesises these ideas by using interpretability tools not just for analysis but as an active component of the training process itself. The goal is to constrain the model, forcing it to base its decisions on correct, human-approved evidence. The work by Ross et al. is a foundational effort in this direction [19]. They proposed penalising the model's input gradients during training. By adding a term to the loss function that suppresses the model's sensitivity to features pre-identified by humans as irrelevant, they could guide the learning process. The primary limitation, however, is the significant overhead of requiring additional human annotations to explicitly mark these irrelevant features. Subsequent research has sought to refine this approach. Shao et al. proposed using an influence function instead of input gradients to trace predictions back to the training data, offering a more robust measure of feature importance [20]. Similarly, Rieger et al. introduced Contextual Decomposition Explanation Penalisation, which incorporates prior knowledge as an explanation error in the loss function, penalising the model if its internal attributions deviate from a desired domain [21]. While powerful, these methods generally rely on the availability of prior knowledge or additional annotations to guide the model.

Our work is similar to this paradigm, but seeks to reduce the need for explicit human supervision of irrelevant features. By using class prototypes as a weak target for the model's attention (as visualised by Grad-CAM), we aim to provide a supervisory signal that is generated from the data distribution itself, creating a more scalable and automated method for training models that learn for the right reasons.

# 3 Methods

The proposed method is tested on the MNIST and FMNIST datasets. The algorithm is an improvement of the Contrastive Loss Approach, proposed in the previous work from which this is derived [7, 8]. The employed approaches in these papers utilise the Grad-CAM algorithm in training to guide image classification towards an extracted feature space (feature map) that is significant, as it matches the supposed relevant part of the images. The gradient-accessing method was based on the hook method, which is inefficient, as discussed in Section 3.3. The reconstruction part of the loss was based on the comparison of the Grad-CAM with the relative input images against the far more generalised prototypes introduced here. The total loss was also composed of a contrastive reconstruction term, in which the input images and the produced Grad-CAM were evaluated with the bi-dimensional Euclidean distance. The total loss was represented in the following equations 1 and 2.

$$L_{\text{contrastive}} = \frac{1}{2} (Y \cdot D^2 + (1 - Y) \cdot \max(m - D, 0)^2)$$
 (1)

Where: Y is a label (1 for similar pairs, 0 for dissimilar pairs); D is the Euclidean distance between the two output tensors; m is the margin (a hyperparameter). The

Multi-Class Cross-Entropy Loss (LCE) can be expressed as:

$$LCE = -\frac{1}{N} \sum_{i=1}^{N} (Y_i \log(p_i) + (1 - Y_i) \log(1 - p_i))$$
 (2)

The loss term proposed in the next section is similar, but without the contrastive part utilised in the previous papers.

#### 3.1 Data

The data are initially analysed using the one-channel approach, and the only data transformation is tensorisation and normalisation to the one-channel MNIST and Fashion MNIST literature values for mean and standard deviation (equal to [0.1307, 0.3081] and [0.2860, 0.3530], respectively). No data augmentation techniques were employed, except resizing the input images as detailed in Section 3.4. The prototypes class images are constructed using the training set and validation set of both datasets. The images are obtained by averaging over these two sets, and the reconstructed prototypes are used separately during the training and validation steps of the model. This method uses the gradient during the validation step, but does not update it, as it should be done only in the training step to avoid contamination errors.

#### 3.2 Model

Three model architectures are tested to benchmark the proposed new algorithms. The first is a baseline CNN that processes an image and flattens its features into a vector before a fully connected layer classifies it into one of the 10 classes of MNIST or Fashion-MNIST. The other two, ResNet18 and ConvNeXt-V2-Tiny, were chosen to assess the algorithms' effectiveness on more advanced architectures known for their potent feature extraction capabilities. ResNet [22] introduces residual connections, while ConvNeXt-V2 introduces techniques as a fully convolutional masked autoencoder (FCMAE) framework and a new Global Response Normalisation (GRN) [1].

## 3.3 Reconstruction GradCAM and Loss

In the first two examples [7, 8] of this proposed training method, reconstruction was performed during the training process, image by image. This was very ineffective, and therefore, the entire reconstruction was redesigned. Instead of analysing each image individually, the Grad-CAM is evaluated at the end of each batch using a vectorisation approach, which, moreover, speeds up the process. The main distinction lies in how and when the gradients are computed and retrieved. The new approach in Algorithm 1 utilises the torch.autograd.grad function, which is a direct and stateless approach. It operates like a specialised tool to request the gradient of a specific output (the target class score) with respect to a particular input (the convolutional feature maps). This technique is notably clean and self-contained, as it doesn't require modifying the model's internal structure by attaching listeners or hooks. Its efficiency often

surpasses that of the alternative because it calculates only the precise information needed, thereby avoiding the computational expense of a complete backwards pass that would generate gradients for every parameter in the model. In contrast, the old method, Algorithm 2, was characterised as a hook-based method that is deeply integrated into the model's class structure. This technique relies on registering hooks, which act as listeners that capture the necessary data during the model's execution. It saves the feature maps during the forward pass and the gradients during the backwards pass. The primary drawback of this design is its operational inefficiency. To obtain the specific gradient for each image, it must perform a separate backwards pass (call) for every item within the batch in a loop. This iterative process is generally less performant, as it retains the computation graph in memory for a more extended period, introducing significant overhead and making it a more complex and resource-intensive solution.

#### Algorithm 1 Functional Grad-CAM Generation (New architecture)

```
procedure GENERATEGRADCAM(L, A)
          Input: Logits L of shape (N, C), Feature Maps A of shape (N, K, H, W)
 2:
 3:
          Output: Batch of Class Activation Maps M_{batch}
          Initialize an empty list cams_list
 4:
          for i=1,\ldots,N do
                                                                 ▶ Iterate through each item in the batch
 5:
               c \leftarrow \arg\max(L_i)
                                                                           ▶ Get index of the predicted class
 6:
              S_c \leftarrow L_{i,c}
G \leftarrow \frac{\partial S_c}{\partial A}
                                                                     ▶ Get the score for the predicted class
 7:
                                                                   ▷ Compute gradients via autograd.grad
 8:
 9:
               \alpha_k^c \leftarrow \frac{1}{H \times W} \sum_{u=1}^H \sum_{v=1}^W G_{i,k,u,v}
                                                                    10:
     for weights
11:
              \begin{aligned} M_i \leftarrow \text{ReLU}\left(\sum_{k=1}^K \alpha_k^c A_{i,k}\right) \\ M_i \leftarrow \frac{M_i - \min(M_i)}{\max(M_i) - \min(M_i)} \\ \text{Append } M_i \text{ to } cams\_list \end{aligned}
                                                               \triangleright Compute weighted sum of feature maps
12:
                                                                                       \triangleright Normalize map to [0, 1]
13:
14:
          end for
15:
          M_{batch} \leftarrow \operatorname{Stack}(\operatorname{cams\_list})
16:
          return M_{batch}
17:
18: end procedure
```

The Loss approach has also been updated so that explanations for all images of the same class should be semantically similar. The model isn't asked to reconstruct the original input image from its CAM. Instead, it's trained to create an explanation for any given class instance that resembles an abstract prototype for that class. The prototype is calculated once at the beginning by averaging all training and validation images belonging to a specific class (e.g., the prototype for a T-shirt, a Number, or a medical condition). The goal is to enforce consistency in what the model is classifying. The two proposed losses are:

#### Algorithm 2 Hook-Based Grad-CAM (Old architecture)

#### Setup:

- 1: Register a forward hook on the target layer to save its output to a global variable A.
- 2: Register a backwards hook on the target layer to save its gradient to a global variable  $\mathcal{G}$ .

```
procedure ModelForwardWithCAM(X)
 4:
          Input: Batch of images X of shape (N, C_{in}, H_{in}, W_{in})
          Output: Logits L and batch of Class Activation Maps M_{batch}
 5:
 6:
          L \leftarrow \text{ModelForward}(X) \triangleright \text{Forward pass triggers hook, storing feature maps in}
 7:
     \mathcal{A}
          Initialize an empty list cams_list
 8:
          for i = 1, \dots, N do
                                                                   ▶ Iterate through each item in the batch
 9:
               c \leftarrow \arg\max(L_i)
10:
               S_c \leftarrow L_{i,c}
11:
               S_c.backward(retain_graph=True) \triangleright Backward pass triggers hook, storing
12:
     gradients in \mathcal{G}
13:
               \alpha_k^c \leftarrow \frac{1}{H \times W} \sum_{u=1}^H \sum_{v=1}^W \mathcal{G}_{i,k,u,v}
                                                                      ▷ Global Average Pooling on gradients
14:
15:
               \begin{aligned} M_i \leftarrow \text{ReLU}\left(\sum_{k=1}^K \alpha_k^c \mathcal{A}_{i,k}\right) \\ M_i \leftarrow \frac{M_i - \min(M_i)}{\max(M_i) - \min(M_i)} \\ \text{Append } M_i \text{ to } \textit{cams\_list} \end{aligned}
                                                                 ▷ Compute weighted sum of feature maps
16:
                                                                                          \triangleright Normalize map to [0, 1]
17:
18:
          end for
19:
          M_{batch} \leftarrow \text{Concatenate}(cams\_list)
20:
          return L, M_{batch}
21:
     end procedure
22:
```

- 1. Prototype Loss (Per-Image Consistency): This loss operates on an individual level. For each image in a batch, it generates a Grad-CAM and calculates the loss between that CAM and the pre-computed prototype for the image's actual class.
- 2. Batch-CAM Prototype Loss (Batch-Level Consistency): This is a more aggregated approach. Instead of generating a CAM for each single image, it computes the average CAM per class present in the batch. It does this by averaging the gradients and feature maps for all instances of that class. This single, batch-averaged CAM is then compared to the class prototype using the loss. This encourages the model to generate consistent explanations for a class at a group level. To evaluate the Batch-CAM for a given class c, the feature maps from all  $N_c$  samples belonging to that class within the batch B are averaged together equation 3, similarly, the gradients of the class score with respect to the feature maps are also averaged across all  $N_c$  samples, Equation 4, lastly The neuron importance weights are then calculated by

applying Global Average Pooling (GAP) to the averaged gradients, Equation 5.

$$\bar{A}_k^c = \frac{1}{N_c} \sum_{i \in \mathcal{B}} A_{i,k} \tag{3}$$

$$\bar{G}_k^c = \frac{1}{N_c} \sum_{i \in \mathcal{B}_c} \frac{\partial S_c}{\partial A_{i,k}} \tag{4}$$

$$\bar{\alpha}_{k}^{c} = \frac{1}{H \times W} \sum_{u=1}^{H} \sum_{v=1}^{W} (\bar{G}_{k}^{c})_{u,v}$$
 (5)

The loss can be formulated using various metrics. Although prior work employed the Euclidean distance (L2 norm) to quantify reconstruction error, we identified this approach as a performance bottleneck. Consequently, this study presents a comparative analysis of the classical L1 and L2 norm-based reconstruction losses and SSIM to determine the most effective loss function for our training paradigm.

#### 1. Structural Similarity Index (SSIM) Loss

This loss is based on the degradation of structural information between two images. It operates on a single scale, combining three key components: luminance (l), contrast (c), and structure (s). The loss is calculated as one minus the SSIM index 6.

$$\mathcal{L}_{SSIM}(x,y) = 1 - [l(x,y)]^{\alpha} \cdot [c(x,y)]^{\beta} \cdot [s(x,y)]^{\gamma}$$
(6)

Where:

- $\bullet$  x and y are the two images being compared.
- l, c, s are the luminance, contrast, and structure comparisons, respectively, Equations [7-9].

$$l(x,y) = \frac{2\mu_x \mu_y + C_1}{\mu_x^2 + \mu_y^2 + C_1} \tag{7}$$

$$c(x,y) = \frac{2\sigma_x \sigma_y + C_2}{\sigma_x^2 + \sigma_y^2 + C_2} \tag{8}$$

$$s(x,y) = \frac{\sigma_{xy} + C_3}{\sigma_x \sigma_y + C_3} \tag{9}$$

The values of  $\mu_{x,y}$  and  $\sigma_{x,y}$  are the image's pixel mean and standard deviation, while the constant term  $C_{1,2,3}$  is a small positive constant to avoid a near-zero error bound.

•  $\alpha, \beta, \gamma$  are weighting parameters to adjust the relative importance of each component.

In our framework, the classification loss is always composed of the Cross-Entropy Loss ( $\mathcal{L}_{\text{Class}}$ ) and one of the three combinations of the Prototype Loss or the Batch-CAM prototype Loss.

If using Prototype Loss (Per-Image Consistency) with a chosen metric (L1, L2, or SSIM), the reconstruction/alignment term would be  $\mathcal{L}_{\text{Proto}}^{\text{Metric}}(M_i, P_c)$ , where  $M_i$  is

the Grad-CAM for image i,  $P_c$  is the prototype for its class c, and 'Metric' denotes L1, L2, or SSIM.

The total loss for this approach is:

$$\mathcal{L}_{\text{Total}} = \lambda_{\text{class}} \mathcal{L}_{\text{Class}} + \lambda_{\text{proto}} \mathcal{L}_{\text{Proto}}^{\text{Metric}}(M, P)$$
 (10)

Where:

- $\mathcal{L}_{\text{Class}}$  is the standard Cross-Entropy Loss for classification.
- $\mathcal{L}_{\text{Proto}}^{\text{Metric}}(M, P)$  represents the chosen metric (L1, L2, or SSIM) applied between the per-image Grad-CAMs (M) and their respective class prototypes (P).
- $\lambda_{class}$  and  $\lambda_{proto}$  are hyperparameters weighting the contribution of each loss component.

If using Batch-CAM Prototype Loss with a chosen metric (L1, L2, or SSIM), the reconstruction/alignment term would be  $\mathcal{L}_{\text{BatchProto}}^{\text{Metric}}(\bar{M}_c, P_c)$ , where  $\bar{M}_c$  is the batch-averaged Grad-CAM for class c, and  $P_c$  is the prototype for that class.

The total loss for this approach is:

$$\mathcal{L}_{\text{Total}} = \lambda_{\text{class}} \mathcal{L}_{\text{Class}} + \lambda_{\text{batch-proto}} \sum_{c \in C_B} \mathcal{L}_{\text{BatchProto}}^{\text{Metric}}(\bar{M}_c, P_c)$$
 (11)

Where:

- $\bullet$   $\mathcal{L}_{Class}$  is the standard Cross-Entropy Loss for classification.
- $\mathcal{L}_{\text{BatchProto}}^{\text{Metric}}(\bar{M}_c, P_c)$  represents the chosen metric (L1, L2, or SSIM) applied between the batch-averaged Grad-CAMs ( $\bar{M}_c$ ) and their class prototypes ( $P_c$ ). The sum is taken over all unique classes present in the current training batch.
- $\lambda_{\text{class}}$  and  $\lambda_{\text{batch\_proto}}$  are hyperparameters weighting the contribution of each loss component.

#### 3.4 Experiments

To test our different training approaches, we conducted a two-stage experiment. In the first stage, we benchmarked three architectures: a Simple CNN, ResNet-18, and ConvNeXt-V2-Tiny on 28x28 images. Each architecture was trained under seven conditions: a baseline using the classical cross-entropy loss, plus three loss variants of both our Prototype Loss and Batch-CAM Prototype Loss. This initial comparison yielded low-resolution Grad-CAMs (14x14 for the CNN, and just 3x3 for the deeper networks).

In the second stage, we took the single best-performing training method for the ResNet-18 and ConvNeXt-V2-Tiny models and retrained them on larger 112x112 images. This enabled us to generate higher-resolution Grad-CAMs for a more nuanced assessment of how spatial dimensions impact the model learning patterns.

#### 4 Results

The power of DL models is clear from the full review of the results obtained through all experiments, as the capacity of classifying the MNIST and F-MNIST datasets is

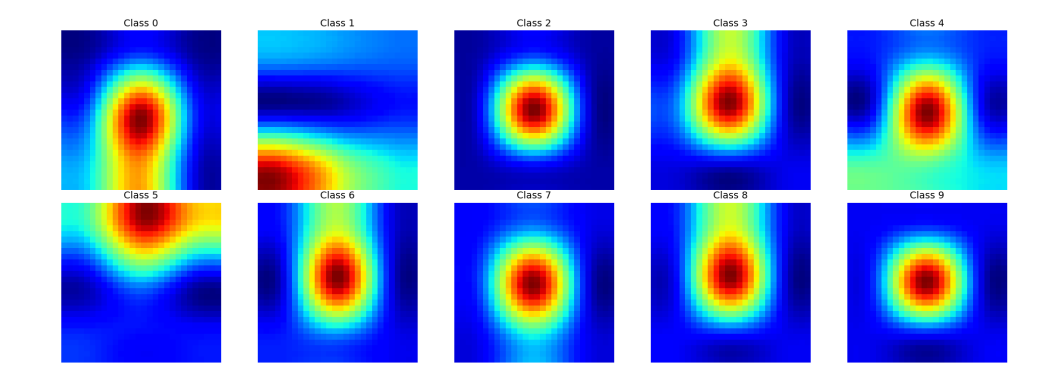


Fig. 2 Average MNIST reconstruction prototypes per class in case of 23x23 images on architecture such as ResNet and ConvNeXt-V2

exceptional and the more complex the architecture the more powerful the model, as table 1 in this one-shot training example ConvNeXt-V2 and ResNet18, exceeds the classification capacity of a simpler neural networks.

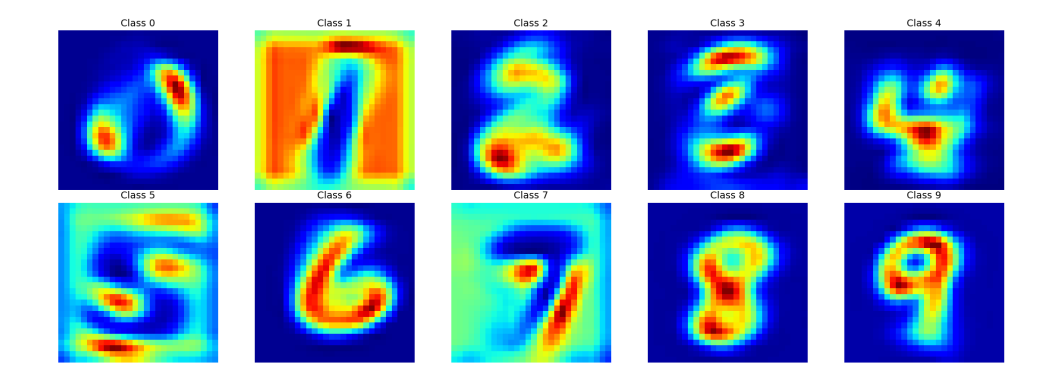
**Table 1** Best accuracy and corresponding experiment for each model. BCPL: Batch-CAMPrototype Loss.

Model	MNI	ST	FashionMNIST		
1,10 401	Experiment	Acc. (%)	Experiment	Acc. (%)	
ConvNeXt-V2 Tiny ResNet18	BCPL_L1 BCPL_L2	99.72 99.65	Baseline BCPL_L2	94.79 94.99	
SimpleCNN	$BCPL_L1$	99.00	BCPL_L1	91.32	

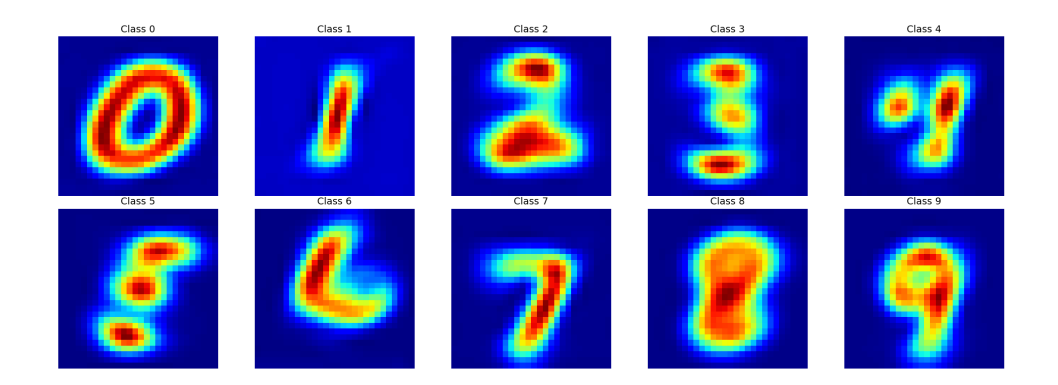
As reported in Appendix A, the number of parameters that the two architectures employ over a simple CNN is enormous with respect to their classification power. A possible drawback is also visible in the reconstruction mechanism; each classic training style model can classify but lacks a conceptual generalisation step, as shown in the figure 2.

In the standard CNN model, the network learns to classify images correctly by capturing a semantic representation of the input. However, due to the significant spatial downsampling in the final layers, the feature maps become too small to permit a faithful reconstruction of the original image. As the Grad-CAM visualisation in Figure 3 demonstrates, the resulting activation map is a low-resolution proxy that is not comparable to the input, even with a correct classification. In contrast, our model, guided by either the Prototype Loss or the Batch-CAM Prototype Loss, achieves a more effective compression that generalises well to the test set, as shown in Figure 4.

The second part of the experiments that use a larger input image size for both ResNet and ConvNeXt-V2 models can perfectly summarise this problem since the bigger available feature maps fed to the fully connected layer achieve higher classification



 ${\bf Fig.~3}~{\rm Average~MNIST~reconstruction~prototypes~per~class~in~case~of~23x23~images~on~architecture~CNN~with~classical~cross-entropy~loss$ 



 ${\bf Fig.~4}~{\rm Average~MNIST~reconstruction~prototypes~per~class~in~case~of~23x23~images~on~architecture~CNN~with~the~Batch-CAM~Prototype~Loss$ 

precision, Table 2 and better capture the details to use to output the classification promptly, Figures  $5\ 6.$ 

 $\begin{tabular}{ll} \textbf{Table 2} & Best model retrained on image size 112x112, which produced feature maps dimensions that are comparable to MNIST and F-MNIST original image size of $28x28$ \end{tabular}$ 

Model	MNIST		FashionMNIST	
	Experiment	Acc. (%)	Experiment	Acc. (%)
ConvNeXt-V2 Tiny ResNet18	BCPL_L1 BCPL_L1	99.74 99.71	BCPL_L1 BCPL_L1	95.01 94.99

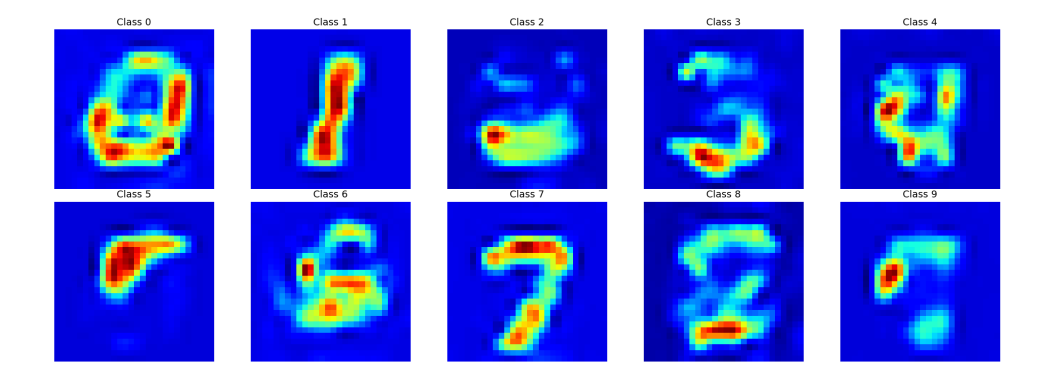


Fig. 5 Average reconstruction prototypes per class in case of MNIST 112x112 images on ConvNeXt-V2 with the Batch-CAM Prototype Loss (L1)

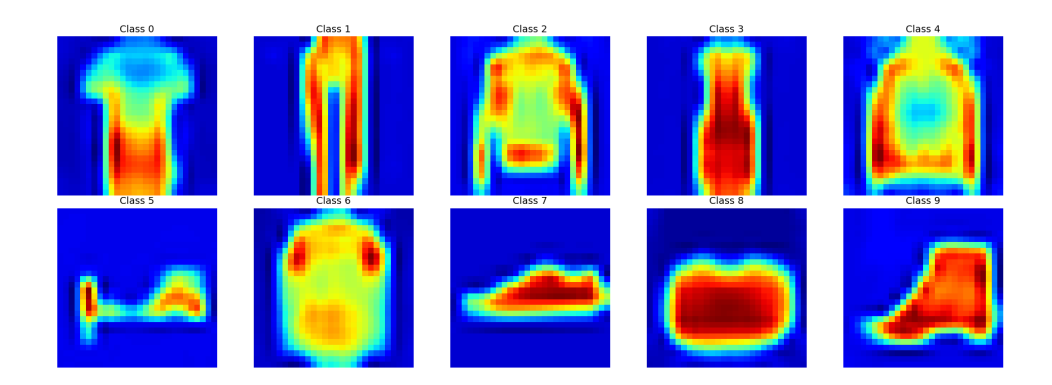


Fig. 6 Average reconstruction prototypes per class in case of of F-MNIST 112x112 images on ConvNeXt-V2 with the Batch-CAM prototype Loss (L1)

#### 5 Conclusion

This paper introduced a novel training paradigm that integrates an explanatory mechanism directly into the model's learning process, shifting the focus from purely predictive accuracy to a more robust learning pattern for the right reasons. By synergising a computationally efficient, batch-wise implementation of Grad-CAM with a prototype-based loss, we have demonstrated a practical method for guiding a model's attention towards semantically meaningful features. Our core contribution lies in leveraging the data's own distribution to generate a supervisory signal, thereby constraining the model to produce explanations that are consistent across instances of the same class

Our empirical evaluation across three distinct CNN architectures (SimpleCNN, ResNet18, and ConvNeXt-V2-Tiny) on the MNIST and Fashion-MNIST datasets confirms the efficacy of this approach. The results indicate not only a consistent

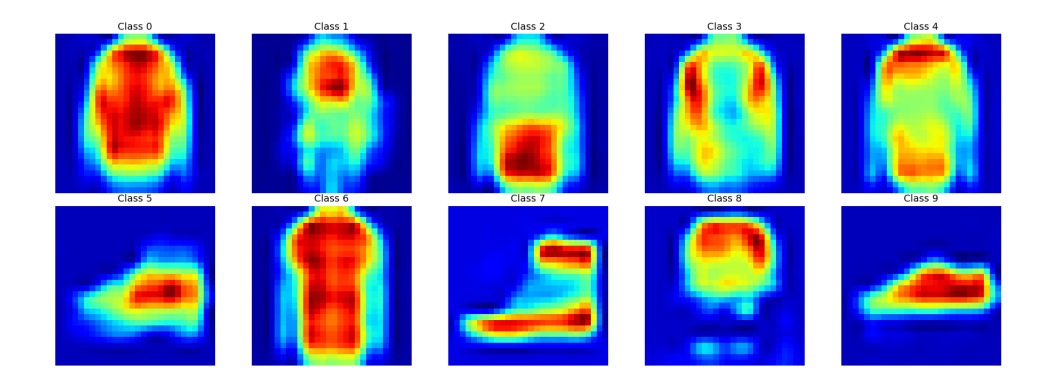


Fig. 7 Average erroneous reconstruction prototypes per class in case of F-MNIST 112x112 images on ConvNeXt-V2 with the Batch-CAM prototype Loss (L1)

improvement in classification accuracy with the proposed Batch-CAM Prototype Loss (BCPL) variants, but also a profound enhancement in the qualitative nature of the model's reasoning. The generated Class Activation Map (CAM) prototypes for models trained with our method exhibit significantly higher coherence and more precise representations of the class-defining features (as illustrated in Figures 4, 5, and 6) compared to the diffuse and often ambiguous CAMs produced by baseline models. This demonstrates that the model is not merely classifying correctly but is building a more robust and generalizable internal concept of each class. Furthermore, analysing reconstructed prototypes from the test set provides a powerful diagnostic tool. For correctly classified images, the prototypes affirm that the model has learned to focus on the expected, human-interpretable features. Conversely, the prototypes generated for misclassified images offer invaluable insight into the model's failure mode, as shown in Figure 7.

They reveal specific points of confusion—for instance, when misclassifying a Pullover (Class 2), the model's focus shifts from the correct activation on the torso and sleeves to a non-descript region at the bottom of the garment. Similarly, the model's confusion with an Ankle boot (Class 9) is evident as its attention ignores the defining ankle structure and instead focuses on the lower shoe profile, a feature it shares with a Sneaker (Class 7). This level of transparency is critical for debugging, identifying dataset biases, and building trust in the model's decisions. The architectural redesign of the Grad-CAM generation, which transitioned from a hook-based method to a direct autograd implementation, drastically reduced computational overhead, making this approach scalable and efficient for practical applications, as can be seen in the table of appendix A, the introduced loss term do not alter the overall numbers of parameters of the model nor the GFLOPs necessary for training it, the few operation introduced in the loss form do not add order of magnitude to the complexity of the model.

While this work establishes a strong proof of concept, the research is limited to a simple image domain. It should be extended to more complex, real-world datasets where spurious correlations are more prevalent and the cost of opaque reasoning is higher, such as in medical imaging or autonomous navigation. Future work could also explore more sophisticated methods for prototype generation beyond simple averaging,

potentially utilising generative models to capture a richer and more varied representation of each class archetype. Ultimately, this research substantiates the principle that explainability should not be an afterthought but a fundamental component of the training objective. By compelling models to justify their predictions in a manner that is human-understandable, we can pave the way for the development of more robust, reliable, and trustworthy artificial intelligence systems.

# Appendix A Overall training results

In this chapter, all the model information of the main experiments is reported in the following Table A1.

 $\begin{tabular}{ll} \textbf{Table A1} & \textbf{Detailed experiment results. BCPL: Batch-CAM Prototype Loss, PL: Prototype Loss.} \end{tabular}$ 

Model	Dataset	Exp.	Acc. (%)	Params (M)	GFLOPs
ConvNeXt-V2 Tiny	FashionMNIST	Baseline	94.79	27.82	0.83
ConvNeXt-V2 Tiny	FashionMNIST	$PL_L2$	94.77	27.82	0.83
ConvNeXt-V2 Tiny	FashionMNIST	$BCPL_L1$	94.59	27.82	0.83
ConvNeXt-V2 Tiny	FashionMNIST	$PL\_SSIM$	94.52	27.82	0.83
ConvNeXt-V2 Tiny	FashionMNIST	BCPL_SSIM	94.45	27.82	0.83
ConvNeXt-V2 Tiny	FashionMNIST	$PL_L1$	94.43	27.82	0.83
ConvNeXt-V2 Tiny	FashionMNIST	$BCPL_L2$	94.36	27.82	0.83
ConvNeXt-V2 Tiny	MNIST	BCPL_L1	99.72	27.82	0.83
ConvNeXt-V2 Tiny	MNIST	Baseline	99.71	27.82	0.83
ConvNeXt-V2 Tiny	MNIST	BCPL_SSIM	99.70	27.82	0.83
ConvNeXt-V2 Tiny	MNIST	$BCPL_L2$	99.68	27.82	0.83
ConvNeXt-V2 Tiny	MNIST	$PL\_SSIM$	99.66	27.82	0.83
ConvNeXt-V2 Tiny	MNIST	$PL_L2$	99.63	27.82	0.83
ConvNeXt-V2 Tiny	MNIST	$PL_L1$	99.47	27.82	0.83
ResNet18	FashionMNIST	$BCPL_L2$	94.99	11.17	0.46
ResNet18	FashionMNIST	$PL\_SSIM$	94.98	11.17	0.46
ResNet18	FashionMNIST	BCPL_SSIM	94.87	11.17	0.46
ResNet18	FashionMNIST	Baseline	94.82	11.17	0.46
ResNet18	FashionMNIST	$PL_L1$	94.81	11.17	0.46
ResNet18	FashionMNIST	BCPL_L1	94.76	11.17	0.46
ResNet18	FashionMNIST	$PL_L2$	94.72	11.17	0.46
ResNet18	MNIST	$BCPL_L2$	99.65	11.17	0.46
ResNet18	MNIST	Baseline	99.61	11.17	0.46
ResNet18	MNIST	$\mathrm{PL} \boldsymbol{.} \mathrm{L2}$	99.61	11.17	0.46
ResNet18	MNIST	$PL\_SSIM$	99.58	11.17	0.46
ResNet18	MNIST	BCPL_SSIM	99.57	11.17	0.46
ResNet18	MNIST	$PL_L1$	99.57	11.17	0.46
ResNet18	MNIST	BCPL_L1	99.49	11.17	0.46
SimpleCNN	${\bf Fashion MNIST}$	$BCPL_L1$	91.32	0.42	0.00
SimpleCNN	FashionMNIST	$BCPL_L2$	91.26	0.42	0.00
SimpleCNN	FashionMNIST	Baseline	91.14	0.42	0.00
SimpleCNN	FashionMNIST	$\mathrm{PL}_{-}\mathrm{L2}$	90.99	0.42	0.00
SimpleCNN	FashionMNIST	$BCPL\_SSIM$	90.94	0.42	0.00
SimpleCNN	FashionMNIST	$PL\_SSIM$	90.91	0.42	0.00
SimpleCNN	FashionMNIST	PL_L1	90.85	0.42	0.00
SimpleCNN	MNIST	BCPL_L1	99.00	0.42	0.00
SimpleCNN	MNIST	$PL_L2$	98.95	0.42	0.00
SimpleCNN	MNIST	Baseline	98.92	0.42	0.00
SimpleCNN	MNIST	$PL\_SSIM$	98.89	0.42	0.00
SimpleCNN	MNIST	$BCPL_L2$	98.87	0.42	0.00
SimpleCNN	MNIST	$PL_L1$	98.75	0.42	0.00
SimpleCNN	MNIST	BCPL_SSIM	98.72	0.42	0.00

# References

[1] Woo, S., Debnath, S., Hu, R., Chen, X., Liu, Z., Kweon, I.S., Xie, S.: Convnext

- v2: Co-designing and scaling convnets with masked autoencoders. In: Proceedings of the IEEE/CVF Conference on Computer Vision and Pattern Recognition, pp. 16133–16142 (2023)
- [2] Dosovitskiy, A., Beyer, L., Kolesnikov, A., Weissenborn, D., Zhai, X., Unterthiner, T., Dehghani, M., Minderer, M., Heigold, G., Gelly, S., et al.: An image is worth 16x16 words: Transformers for image recognition at scale. arXiv preprint arXiv:2010.11929 (2020)
- [3] Ye, W., Zheng, G., Cao, X., Ma, Y., Zhang, A.: Spurious correlations in machine learning: A survey. arXiv preprint arXiv:2402.12715 (2024)
- [4] Bubeck, S., Chandrasekaran, V., Eldan, R., Gehrke, J., Horvitz, E., Kamar, E., Lee, P., Lee, Y.T., Li, Y., Lundberg, S., et al.: Sparks of artificial general intelligence: Early experiments with gpt-4. arXiv preprint arXiv:2303.12712 (2023)
- [5] Bodria, F., Giannotti, F., Guidotti, R., Naretto, F., Pedreschi, D., Rinzivillo, S.: Benchmarking and survey of explanation methods for black box models. Data Mining and Knowledge Discovery 37(5), 1719–1778 (2023) https://doi.org/10. 1007/s10618-023-00933-9
- [6] Zhao, W.X., Zhou, K., Li, J., Tang, T., Wang, X., Hou, Y., Min, Y., Zhang, B., Zhang, J., Dong, Z., et al.: A survey of large language models. arXiv preprint arXiv:2303.18223 1(2) (2023)
- [7] Ignesti, G., Moroni, D., Martinelli, M.: You've got the wrong number: evaluating deep learning training paradigms using handwritten digit recognition data. Pattern Recognition and Image Analysis **34**(4) (2024). In press
- [8] Ignesti, G., Martinelli, M., Moroni, D.: You've got the wrong outfit: Evaluating deep learning paradigms on digit and fashion recognition. In: International Conference on Pattern Recognition, pp. 202–215 (2024). Springer
- [9] Selvaraju, R.R., Cogswell, M., Das, A., Vedantam, R., Parikh, D., Batra, D.: Grad-cam: Visual explanations from deep networks via gradient-based localization. In: Proceedings of the IEEE International Conference on Computer Vision, pp. 618–626 (2017)
- [10] Terven, J., Cordova-Esparza, D.-M., Romero-González, J.-A., Ramírez-Pedraza, A., Chávez-Urbiola, E.A.: A comprehensive survey of loss functions and metrics in deep learning. Artificial Intelligence Review 58(7), 195 (2025) https://doi.org/10.1007/s10462-025-11198-7
- [11] Foret, P., Kleiner, A., Mobahi, H., Neyshabur, B.: Sharpness-aware minimization for efficiently improving generalization. arXiv preprint arXiv:2010.01412 (2020)

- [12] Siméoni, O., Vo, H.V., Seitzer, M., Baldassarre, F., Oquab, M., Jose, C., Khalidov, V., Szafraniec, M., Yi, S., Ramamonjisoa, M., et al.: Dinov3. arXiv preprint arXiv:2508.10104 (2025)
- [13] Raissi, M., Perdikaris, P., Karniadakis, G.E.: Physics informed deep learning (part i): Data-driven solutions of nonlinear partial differential equations. arXiv preprint arXiv:1711.10561 (2017)
- [14] Karniadakis, G.E., Kevrekidis, I.G., Lu, L., Perdikaris, P., Wang, S., Yang, L.: Physics-informed machine learning. Nature Reviews Physics 3(6), 322–340 (2021)
- [15] Ribeiro, M.T., Singh, S., Guestrin, C.: "why should i trust you?" explaining the predictions of any classifier. In: Proceedings of the 22nd ACM SIGKDD International Conference on Knowledge Discovery and Data Mining, pp. 1135–1144 (2016)
- [16] Chattopadhay, A., Sarkar, A., Howlader, P., Balasubramanian, V.N.: Grad-cam++: Generalized gradient-based visual explanations for deep convolutional networks. In: 2018 IEEE Winter Conference on Applications of Computer Vision (WACV), pp. 839–847 (2018). IEEE
- [17] Chen, C., Li, O., Tao, D., Barnett, A., Rudin, C., Su, J.K.: This looks like that: deep learning for interpretable image recognition. Advances in neural information processing systems **32** (2019)
- [18] Hoffmann, A., Fanconi, C., Rade, R., Kohler, J.: This looks like that... does it? shortcomings of latent space prototype interpretability in deep networks. arXiv preprint arXiv:2105.02968 (2021)
- [19] Ross, A.S., Hughes, M.C., Doshi-Velez, F.: Right for the right reasons: Training differentiable models by constraining their explanations. arXiv preprint arXiv:1703.03717 (2017)
- [20] Shao, X., Skryagin, A., Stammer, W., Schramowski, P., Kersting, K.: Right for better reasons: Training differentiable models by constraining their influence functions. In: Proceedings of the AAAI Conference on Artificial Intelligence, vol. 35, pp. 9533–9540 (2021)
- [21] Rieger, L., Singh, C., Murdoch, W., Yu, B.: Interpretations are useful: penalizing explanations to align neural networks with prior knowledge. In: International Conference on Machine Learning, pp. 8116–8126 (2020). PMLR
- [22] He, K., Zhang, X., Ren, S., Sun, J.: Deep residual learning for image recognition. In: Proceedings of the IEEE Conference on Computer Vision and Pattern Recognition, pp. 770–778 (2016)